RSC Advances

ROYAL SOCIETY OF CHEMISTRY

www.rsc.org/advances

Cite this: DOI: 10.1039/c0xx00000x

www.rsc.org/xxxxxx

ARTICLE TYPE

Template Free Synthesis of Porous Boron Nitride Using a Single Source Precursor

Mahdi Maleki,*[a] Ali Beitollahi *[a] and Mohamadreza Shokohimehr[b]

Received (in XXX, XXX) Xth XXXXXXXXX 20XX, Accepted Xth XXXXXXXXX 20XX

DOI: 10.1039/b000000x

Porous boron nitride (BN) powder was prepared through a facile template free synthesis route through the pyrolysis of controlled polymerized ammonia borane (AB) at 1300 °C. The prepared products were characterized using different techniques such as X-ray diffraction technique, X-ray photoelectron spectroscopy, scanning transmission electron microscopy, transmission electron microscopy and N_2 sorption analysis. We investigated the effect of AB polymerization temperature and time on the micropores formation and surface area of the obtained products. The lower heating temperature of AB before pyrolysis resulted in higher surface area and pore volume and micropore volume. The highest surface area was obtained for the isothermal heating of AB at 70 ℃ and 32 h before being subjected to pyrolysis at 1300 ℃.

.

1. Introduction

The formation of micropores in the organic or inorganic porous structures can be created by different methods. It is already shown that removing the organic templates such as polystyren-b-polyethyleneoxide (PS-b-PEO), Pluronic P123 and quaternary ammonium salts can generate micropores in the porous materials.[1-4] For instance, mutually interpenetrating network of an inorganic precursor and hydrophilic PEO chains in PS-b-PEO led to the micropores formation.[1] Furthermore, small organic compounds such as quaternary alkyl ammonium salts have been used as structure directing agents in the synthesis of zeolite to make a pore network.[2] Another route to obtain the microporous structures is applying molecular assembly of polymers in intrinsic microporous polymers.[5] Synthesis of microporous polymers with rigid and contorted macromolecular structures which cannot fill space efficiently leaving voids in microporous polymers.[5]

Micro/meso porous boron nitride (BN) nanostructure is one of the interesting ceramic materials that has recently paid intensive attentions due to their wide application potentials.[6-8] To date, various procedures have been reported to fabricate nanoporous BN including hard and soft template methods for controlling pore size and shapes of the BN products. [9-13] However, template removal and frequent replications for the hard template methods and complicated approaches for the soft template procedures make them very impractical and inappropriate techniques to obtain nanoporous BN. Therefore, it is an important issue to develop economical and facile approaches for preparing porous BN nanostructures. Template free methods have exhibited a new window in the facile synthesis of porous BN powders.[14-16] In addition, Free template procedure utilizing a single precursor polymerization in special solvents has lend itself as an interesting route for the synthesis of some nanoporous materials such as aluminosilicates.[17, 18] T.T. Borek *et al* has reported the synthesis of microporous BN with single source and template free procedure by polymerization of BN polymeric precursor.[19] However, in this work, the usage of the air sensitive and non-commercially available precursors could be considered as the disadvantage of such preparation route.

Ammonia borane (AB), a white crystalline solid, was first prepared by Shore and Parry.[20] AB is an appropriate precursor for the synthesis of BN structures due to its high contents of B and N and no oxygen and carbon. Although AB has polymerization ability, it has been frequently used for the synthesis of BN nanostructures through chemical vapor deposition methods and less attention has been paid for the BN production through the AB thermal decomposition.[21-23] X. Wang *et al.* has reported synthesis of BN nanosheets through a controlled activation of AB precursor followed by a precise pyrolyzed program.[24] They obtained crystalline BN nanosheets with a low specific surface area (130 m^2 g^{-1}). Herein, we report a facile synthesis of microporous/mesoporous BN nanostructures through a template free method through controlled polymerization of a single source precursor (AB).

2. Experimental

2.1. Chemicals

Ammonia borane complex (97%) was purchased from Sigma–Aldrich company.

2.2. AB polymerization

0.2 g of AB powder was polymerized at 70, 80, 90 °C and 140 °C under N_2 atmosphere in glass vial (Fig. S1). Then, polymerized AB powders were pyrolyzed using heating program 1°C/min ramp to 200 °C (for 2h) followed by 1.4 °C/min ramp to 1150 °C under ammonia atmosphere and 1.4 °C/min to 1300 °C (for 5 min) under N_2 atmosphere based on TGA/DSC results. The samples are named according to the abbreviations and applied reaction conditions with temperature and time. The polymerized and pyrolyzed samples are started with AB and BN, respectively. The details conditions of the prepared samples are shown in table 1.

Table 1 Details conditions of the polymerized and pyrolyzed samples.

Sample	$T_{polymerization}$ (°C)	$t_{polymerization}$ (h)	$T_{heat\ treatment}$ (°C)	$t_{heat\ treatment}$ (min)
AB.70. 32h	70	32	-	-
AB.80. 16h	80	16	-	-
AB.80. 32h	80	32	-	-
AB.90. 16h	90	16	-	-
AB.140.R	140	2	-	-
BN.13.70. 32h	70	32	1300	5
BN.13.80. 16h	80	16	1300	5
BN.13.80. 32h	80	32	1300	5
BN.13.90. 16h	90	16	1300	5
BN.13.140.R	140	2	1300	5

2.3. Characterization

Powder X-ray diffractions (XRD) were obtained using an X'Pert Pro MPD diffractometer (Philips, CuKα, 1.54 °A). Fourier-transformed infrared (FT-IR) spectra were recorded on a PerkinElmer spectrophotometer between 500 and 4000 cm^{-1} using KBr pellets. X-ray photoelectron spectroscopy (XPS) measurements were carried out for the BN powders using an Al Ka source (Sigma probe, VG Scientifics). The carbonaceous C 1s line (284.8 eV) was used as the reference to calibrate the binding energies. Nitrogen physisorption was measured using a Belsorb system at -196 °C. The samples were degassed at 150°C before measurements. The Brunauer–Emmett–Teller (BET) method was utilized to calculate the specific surface area (S_{BET}) using the adsorption branch. The total pore volume (V_P) was estimated from the adsorbed amount at relative pressure of 0.995. The Dubinin−Raduskevitch (DR) theory was used to estimate micropore volume. Transmission electron microscope (TEM) images were obtained using a JEOL EM-2010 microscope at an acceleration voltage of 200 kV. High resolution TEM (HRTEM) images were acquired using a JEOL JEM-3010 microscope at an acceleration voltage of 200 kV. Scanning transmission electron microscopy (STEM) images were obtained using a JEOL JEM-3000F. Thermogravimetric analysis was performed using a SDT Q600 V8.1 Build 99 instrument at heating rates 10°C/min under N_2 atmosphere (flow rate of 100 ml/min).

3. Results and discussion

3.1. Polymerization of AB

To gain better understanding of the AB polymerization behaviour, the physical changes of AB powders during heating at 80, 90 and 140 °C were monitored by visual inspections (Fig. S2). While continuous heating of AB to 140 °C, the melting occurred at 108 °C which is consistent with the TGA/DSC results (Fig. S3). The precursor melting accompanied with hydrogen evolution led to foaming and swelling. The volume of AB increased approximately more than 10 times of the initial volume.

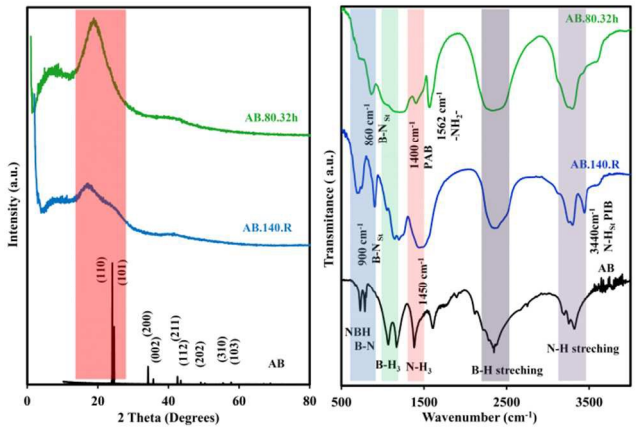

Fig. 1 XRD and FTIR spectra of AB, AB.140.R and AB.80.32h samples.

Similar voluminous swelling properties have been reported by other research groups during the AB heating.[25, 26] After the completion of AB melting, the progress of swelling stopped and volume of the foam powders decreased slightly. At the isothermal heating of AB at 90 °C (AB.90.16h), melting and swelling occurred after 2 h heating. As the hydrogen evolution is an exothermic reaction [27], the released heat could provide the required energy for the AB melting before reaching to its melting point. However, the volume of swelled powders at 90 °C is less than the continuous heating. At the isothermal heating of AB at 70 and 80°C, there was not any observable change in the physical properties of the heated AB powders even after 32 h.

Further characterizations such as XRD and FT-IR were used to study the AB decomposition products under rapid and isothermal heating conditions.

The XRD patterns of AB.80.32h and AB.140.R compared to AB are shown in Fig. 1. The XRD spectrum of AB revealed peaks at 24, 24.5, 34.2, 35.7, 42.6, 43.5, 49.2, 55.4 and 57.7 degrees. The observed peaks are attributed to (110), (101), (200), (002), (211), (112), (202), (310) and (103) reflections in tetragonal structure of AB (JCPDS Card No. 13- 0292). As it can be seen in the Fig. 1, after polymerization of AB at 80 °C (AB.80.32h), all AB peaks disappeared and a new shoulder was formed between 19-21 degrees. The appearance of such a shoulder could be the sign of polyaminoborane (PAB) formation as a main product of AB decomposition.[25] The XRD pattern of AB.140.R also revealed an amorphous structure with lower reflections compared to the AB.80.32h sample. These distinctions are due to the different decomposition products due to different

decomposition routes and temperature.

The FT-IR spectra comparison of AB and AB.140.R revealed that the N-H bonds have shifted and splitted into a higher wavenumber for AB.140.R (Fig. 1). The appearance of a peak at 3435 cm^{-1} demonstrated the presence of the double bond between nitrogen and hydrogen. This could be attributed to polyiminoborane (PIB) formation. Furthermore, Peak of 1450 cm^{-1} in AB.140.R sample is resulted from the net-shaped compounds similar to polyborazines.[28] In addition, the presence of the B-H bond in a higher wavenumber could be another reason for the formation of PIB liked product in the rapid heating.[29] In the sample AB.80.32h, the peaks of the N-H peaks were moved to lower wavenumbers and become broader relative to AB peaks. The presence of a peak at 1562 cm^{-1} could be due to $-NH_2-$ oligomers of PAB.[30] The peak of 1400 cm^{-1} obtained in AB.80.32h sample is assigned to PAB.[29] Therefore, the most probable product is PAB in the isothermal heating process while in the rapid heating procedure the net-shaped products were formed in addition to the PAB product.

3.2. BN formation

Fig. 2 demonstrates the XRD patterns of BN.13.140.R and BN13.80.32h samples revealing the existence of two broad peaks around 20-28 and 40-45 degrees. These peaks are assigned to (002) and (10) in t-BN structure, respectively.[10]

As can be noticed from Fig. 2, slightly higher crystallinity could be obtained for the sample already subjected to polymerization at 140 °C (BN13.140.R sample). Different polymer products resulted from the AB decomposition may cause these changes. It has been reported that the BN precursors with cyclic-shaped structures have memory effect in the formation of highly crystalline BN.[29] Moreover, the presence of highly disordered structures due to presence of micropores could be also possibly responsible for this effect that will be considered later.

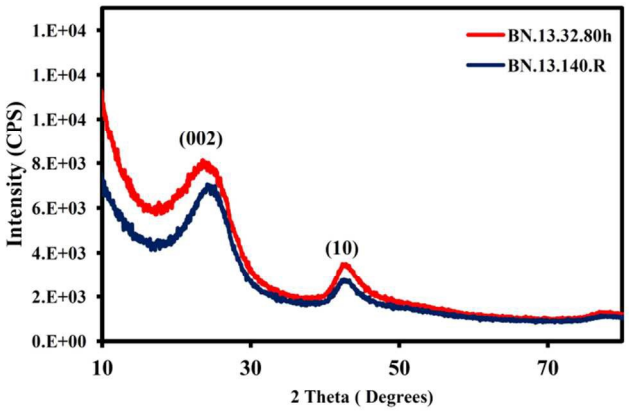

Fig. 2 XRD patterns of BN.13.140.R and BN.13.80.32h samples.

To further investigate the chemical states of the prepared powders, XPS analysis was used for the sample BN.13.80.32h. Fig.3 shows the survey scan, B 1s and N 1s spectra of the prepared powder. The full survey scan spectrum revealed the

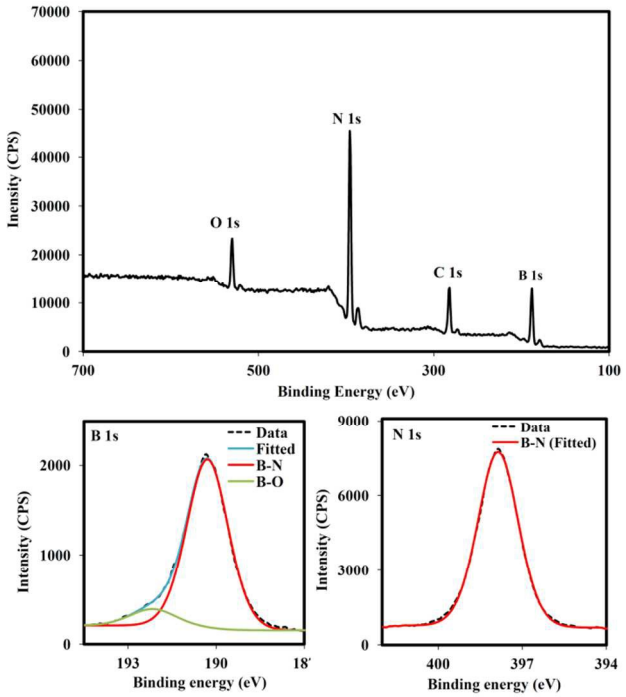

Fig. 3 B 1s, N 1s and survey scan XPS spectra of the sample BN.13.80.32h.

presence of boron, carbon, nitrogen and oxygen in the sample. Since the AB does not have oxygen and carbon, the appearance of such elements in the spectrum could be due to the surface contaminations of pyrolyzed sample during the exposure to the air before the analysis. Further reason for the presence of O element could be attributed to oxidation of polymerized AB during transferring to the furnace. However, as PAB is stable in the air[30], this reason is not most likely. The B 1s spectrum was fitted with two curves using a Gaussian profile. The main one with a binding energy peak at ~190.29 eV is assigned to B-N bonds and the other one at~191.81 eV is attributed to B-O bond.[15, 31] Owing to higher electronegativity of oxygen than nitrogen, this bonding configuration led to the shift of peak to higher binding energies. The N 1s peak revealed a symmetrical Gaussian line shape which peaked at 398.3 eV. Both the B 1s and the N 1s spectra indicate that the configuration for B and N atoms is the B-N bond, implying the BN formation.[15]

2.4. Surface area of the prepared BN powders

N_2 sorption isotherms of the pyrolyzed samples are depicted in Fig. 4. The isotherm of BN.13.140.R and BN.13.90.16h samples could be categorized as type II isotherm that is the characteristic of macroporous materials. The polymerized samples at 70 and 80 °C have type I adsorption isotherm approximately that is assigned to microporous powders. The appearance of hysteresis is due to presence of mesopores in the synthesized samples. Decreasing the polymerization temperature before pyrolysis led to rise of N_2 uptake at low relative pressure below 0.05. This is the sign of increased the level of micropores by the lower polymerization

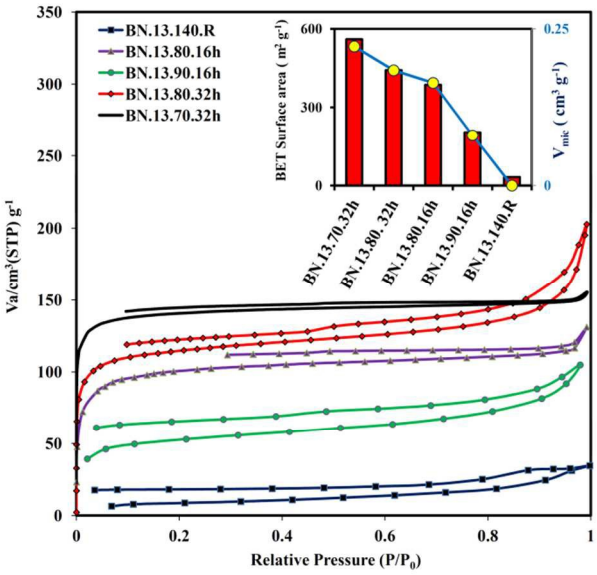

Fig. 4 Nitrogen adsorption-desorption isotherm of the pyrolyzed samples. The inset is the summary of BET surface areas and V_{mic} for the obtained samples.

temperature. Moreover, a higher N_2 uptake at low relative pressure was obtained for the longer polymerization time (32 h) compared to 16 h at 80°C. These observations are consistent with derived data from isotherms in table 2. Decreasing the polymerization temperature enhanced the S_{BET} and V_p and V_{micro}. The highest S_{BET} (560 m^2 g^{-1}), V_P (0.245 cm^3 g^{-1}) and V_{micro} (0.222 cm^3 g^{-1}) were obtained at lowest polymerization temperature of 70 °C (BN13.70.32h). This high surface area is comparable with some report related to synthesis of porous BN through hard template methods. [32, 33] High surface area BN powders (437-712 m^2 g^{-1}) were prepared using single source of BN polymeric precursors.[34] However, synthesis of such air sensitive polymeric precursors (borazine compounds) that are not commercially available is a main constrain for such preparation approach.

Table 2 Pore parameters derived from the nitrogen isotherms for the synthesized samples.

Sample	S_{BET}	V_{total}	V_{micro}
BN.13.70.32h	562.6	0.245	0.222
BN.13.80.16h	386	0.2	0.164
BN.13.80. 32h	442	0.31	0.184
BN.13.90.16h	204	0.162	0.08
BN.13.140.R	31.6	0.005	-

3.4. Morphology of the obtained BN powders

TEM images of the BN.13.90.16h, BN.13.80.32h and BN.13.70.32h samples are shown in Fig. 5. TEM image of BN.13.90.16h sample do not revealed the existence of the noticeable level of micropores as confirmed by BET results as well (Fig. 5a ,b). However, STEM image of this sample in Fig. 5c demonstrated the presence of mesoporoes in the powders. Formation of this mesopores could be due to the second step of hydrogen evolution. TEM images of BN.13.80.32h sample in Fig. 5d, e confirm the formation of mesoporous and microporous. However, both mesopores and micropores in these samples have disordered morphologies. The sample of BN.13.70.32h a revealed

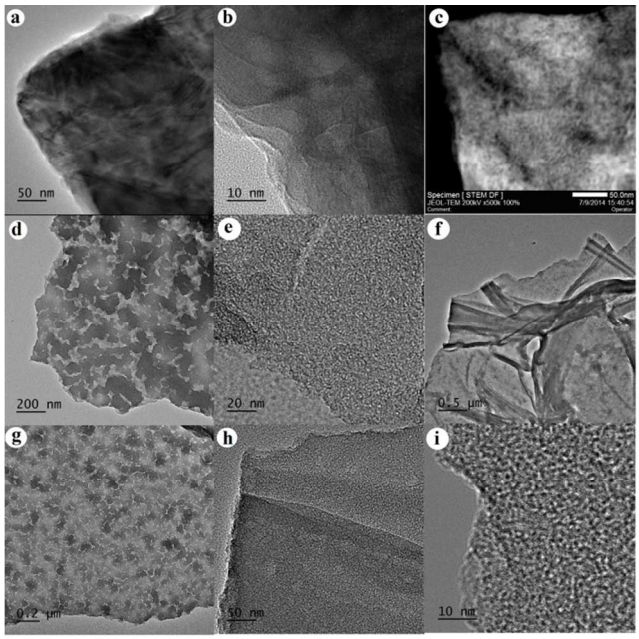

Fig. 5 a) TEM, b) HRTEM and C) STEM images of sample BN.13..90.16h. d) TEM and e) HRTEM images of sample BN.13.80.32h. f, g) TEM and h, i) HRTEM images of sample BN.13.70.32h.

sheet like morphology (Fig. 5f) similar to the result reported by X. Wang group.[24, 35] The formation of sheet like morphology was related to PAB bubbles. But, the TEM image of BN.13.70.32h sample at a higher magnification also revealed the presence of big pores and wormlike micropores (Fig. 5g, h). Stack atomic layers of BN could be detected in micropores walls as shown in Fig. 5h. Such very small crystalline domain could be responsible for appearance of the observed broad XRD reflections at lower degrees compared to crystalline h-BN.

2.5. Micropores formation

P. R. Malenfant *et al* reported using a BN precursor with polymerization ability could lead to formation of micropores powders.[9] D. M. Smith *et al* synthesized a porous BN with a high surface area through vacuum pyrolysis of (poly (4,6-borazinylamine).[19, 34] They used low In addition, pyrolysis of supercritical dried gel containing a poly(borazinylamine) and tetrahydrofuran led to formation BN aerogel.[36] The mechanism of AB decomposition has been extensively explored by other research groups. The overall BN formation from AB decomposition is shown in Fig. 6. As it can be seen the first step of AB decomposition is formation of PAB followed by PIB and BN. This critical step between AB and PAB was considered properly by W. J. Shaw group.[37] X. Wang has also reported this step has critical role in the formation of BN nanosheets.[35] T. Autrey *et al* stated that the decomposition of AB started with disruption of dehydrogen bonding and formation of mobile phase (Fig. 6).[37] Diammoniate of diborane (DADB) is nucleated form AB mobile phase. After that, DADB reacts with remaining AB to form linear chains. By passing the time, linear chains connects together.[37]

As it was mentioned in this work, the most probable product in isothermal heating could be linear polymeric of PAB while at rapid heating cyclic-like products could possibly have been formed.

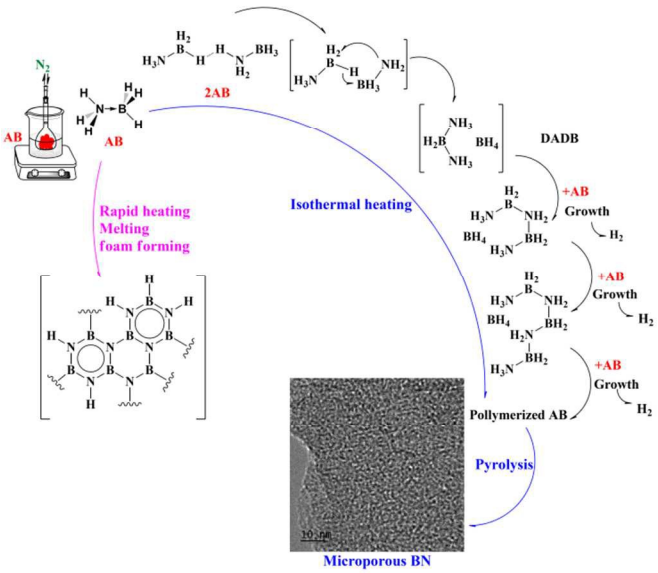

Fig. 6 Schematic presentation of thermal decomposition of AB.[38, 39]

In the so long isotherm heating, the growth and connection of this linear polymeric chain leaves the space between the long linear chains. This inter-space voids probably act as backbone of micropores. Further, in rapid heating, linear chain of AB does not have enough time to further polymerization and melting occurrence disrupt the probable micropores backbones. Of course, further detailed characterization is required to support such assumption.

3. Conclusion

In summary, pyrolysis of controlled polymerized AB at 1300 °C led to formation of high surface area microporous BN powder. Polymerization of AB before pyrolysis has a critical role in micropores formation. The lower temperature heating of AB before pyrolysis resulted in higher surface area and pore volume and micropore volume. The highest surface area was obtained for the heating of AB at 70 °C and 32 h before pyrolysis at 1300 °C.

Notes and references

[a] Center of Excellence for Ceramic Materials in Energy and Environment Applications, School of Metallurgy & Materials Engineering, Iran University of Science and Technology (IUST), Narmak, Tehran 16846, Iran. E-mail: malekim@metaleng.iust.ac.ir; beitolla@iust.ac.ir; Fax: +98 21 77240480; Tel: +98 21 77459151

[b] School of Chemical and Biological Engineering, College of Engineering, Seoul National University, Seoul 151-744, Republic of Korea.

† *Electronic Supplementary Information (ESI) available: [details of any supplementary information available should be included here]. See DOI: 10.1039/b000000x/*

‡ Footnotes should appear here. These might include comments relevant to but not central to the matter under discussion, limited experimental and spectral data, and crystallographic data.

1. B. Smarsly, G. Xomeritakis, K. Yu, N. Liu, H. Fan, R. A. Assink, C. A. Drewien, W. Ruland and C. J. Brinker, *Langmuir*, 2003, **19**, 729.
2. R. Kore and R. Srivastava, *RSC Advances*, 2012, **2**, 10072.
3. A. Galarneau, H. Cambon, F. Di Renzo, R. Ryoo, M. Choi and F. Fajula, *New Journal of Chemistry*, 2003, **27**, 73.
4. C. M. Yang, B. Zibrowius, W. Schmidt and F. Schüth, *Chemistry of Materials*, 2004, **16**, 2918.
5. J. Vile, M. Carta, C. G. Bezzu and N. B. McKeown, *Polymer Chemistry*, 2011, **2**, 2257.
6. Q. Weng, B. Wang, X. Wang, N. Hanagata, X. Li, D. Liu, X. Wang, X. Jiang, Y. Bando and D. Golberg, *ACS Nano*, 2014, **8**, 6123.
7. Q. Weng, X. Wang, C. Zhi, Y. Bando and D. Golberg, *ACS Nano*, 2013, **7**, 1558.
8. W. Lei, D. Portehault, D. Liu, S. Qin and Y. Chen, *Nat Commun*, 2013, **4**, 1777.
9. P. R. Malenfant, J. Wan, S.T.Taylor and M. Manoharan, *Nat Nano*, 2007, **2**, 43.
10. P. Dibandjo, L. Bois, F. Chassagneux, D. Cornu, J.-M. Letoffe, B. Toury, F. Babonneau and P. Miele, *Advanced Materials*, 2005, **7**, 571.
11. M. Maleki, A. Beitollahi, J. Javadpour and N. Yahya, *Ceramics International*, 2015, **41**, 3806.
12. M. Maleki, A. Beitollahi, J. Lee, M. Shokouhimehr, J. Javadpour, E. J. Park, J. Chun and J. Hwang, *RSC Advances*, 2015, **5**, 6528.
13. M. Maleki, A. Beitollahi and M. Shokouhimehr, *European Journal of Inorganic Chemistry*, 2015, n/a.
14. Q. Weng, X. Wang, Y. Bando and D. Golberg, *Advanced Energy Materials*, 2014, **4**, 1301525.
15. D. Liu, W. Lei, S. Qin and Y. Chen, *Sci. Rep.*, 2014, **4**.
16. H. Zhao, X. Song and H. Zeng, *NPG Asia Mater*, 2015, **7**, e168.
17. A. Lemaire and B. L. Su, *Microporous and Mesoporous Materials*, 2011, **142**, 70.
18. A. Lemaire and B.-L. Su, *Langmuir*, 2010, **26**, 17603.
19. T. T. Borek, W. Ackerman, D. W. Hua, R. T. Paine and D. M. Smith, *Langmuir*, 1991, **7**, 2844.
20. S. G. Shore and R. W. Parry, *Journal of the American Chemical Society*, 1955, **77**, 6084.
21. A. Pakdel, C. Zhi, Y. Bando, T. Nakayama and D. Golberg, *ACS Nano*, 2011, **5**, 6507.
22. J. Yu, L. Qin, Y. Hao, S. Kuang, X. Bai, Y.-M. Chong, W. Zhang and E. Wang, *ACS Nano*, 2010, **4**, 414.
23. K. K. Kim, A. Hsu, X. Jia, S. M. Kim, Y. Shi, M. Hofmann, D. Nezich, J. F. Rodriguez-Nieva, M. Dresselhaus, T. Palacios and J. Kong, *Nano Letters*, 2011, **12**, 161.
24. X. Wang, C. Zhi, L. Li, H. Zeng, C. Li, M. Mitome, D. Golberg and Y. Bando, *Advanced Materials*, 2011, **23**, 4072.
25. U. B. Demirci, S. Bernard, R. Chiriac, F. Toche and P. Miele, *Journal of Power Sources*, 2011, **196**, 279.
26. R. Chiriac, F. Toche, U. B. Demirci, O. Krol and P. Miele, *International Journal of Hydrogen Energy*, 2011, **36**, 12955.
27. Y. Zhao, J. Zhang, D. L. Akins and J. W. Lee, *Industrial & Engineering Chemistry Research*, 2011, **50**, 10024.
28. M. R. Weismiller, S. Q. Wang, A. Chowdhury, S. T. Thynell and R. A. Yetter, *Thermochimica Acta*, 2013, **551**, 110.
29. D. P. Kim, K.-T. Moon, J.-G. Kho, J. Economy, C. Gervais and F. Babonneau, *Polymers for Advanced Technologies*, 1999, **10**, 702.

30. R. Komm, R. A. Geanangel and R. Liepins, *Inorganic Chemistry*, 1983, **22**, 1684.
31. C. Guimon, D. Gonbeau, G. Pfister-Guillouzo, O. Dugne, A. Guette, R. Naslain and M. Lahaye, *Surface and Interface Analysis*, 1990, **16**, 440.
32. P. Dibandjo, F. Chassagneux, L. Bois, C. Sigala and P. Miele, *Journal of Materials Chemistry*, 2005, **15**, 1917.
33. S. Schlienger, J. Alauzun, F. Michaux, L. Vidal, J. Parmentier, C. Gervais, F. Babonneau, S. Bernard, P. Miele and J. B. Parra, *Chemistry of Materials*, 2011, **24**, 88.
34. J. F. Janik, W. C. Ackerman, R. T. Paine, D. W. Hua, A. Maskara and D. M. Smith, *Langmuir*, 1994, **10**, 514.
35. X. Wang, A. Pakdel, C. Zhi, K. Watanabe, T. Sekiguchi, D. Golberg and Y. Bando, *Journal of Physics: Condensed Matter*, 2012, **24**, 314205.
36. D. A. Lindquist, T. T. Borek, S. J. Kramer, C. K. Narula, G. Johnston, R. Schaeffer, D. M. Smith and R. T. Paine, *Journal of the American Ceramic Society*, 1990, **73**, 757.
37. W. J. Shaw, M. Bowden, A. Karkamkar, C. J. Howard, D. J. Heldebrant, N. J. Hess, J. C. Linehan and T. Autrey, *Energy & Environmental Science*, 2010, **3**, 796.
38. A. C. Stowe, W. J. Shaw, J. C. Linehan, B. Schmid and T. Autrey, *Physical Chemistry Chemical Physics*, 2007, **9**, 1831.
39. S. Bernard and P. Miele, *Materials Today*, 2014, **17**, 443.